Observation of field-dependent magnetic parameters in the magnetic molecule {Ni$_4$Mo$_{12}$}

Jürgen Schnack* and Mirko Brüger

Universität Osnabrück, Fachbereich Physik, D-49069 Osnabrück, Germany

Marshall Luban, Paul Kögerler, Emilia Morosan, and Ronald Fuchs

Ames Laboratory & Department of Physics and Astronomy, Iowa State University, Ames, Iowa 50011, USA

Robert Modler

Johann Modler GmbH, Postfach 100462, D-63741 Aschaffenburg, Germany

Hiroyuki Nojiri

Institute for Materials Research, Tohoku University, Katahira 2-1-1, Sendai 980-8577, Japan

Ram C. Rai, Jinbo Cao, and Janice L. Musfeldt

Department of Chemistry, University of Tennessee, Knoxville, TN 37996, USA

Xing Wei

National High Magnetic Field Laboratory, Florida State University, Tallahassee, FL, 32310
(Dated: December 14, 2005)

We investigate the bulk magnetic, electron paramagnetic resonance, and magneto-optical properties of {Ni$_4$Mo$_{12}$}, a magnetic molecule with antiferromagnetically coupled tetrahedral Ni^{II} in a diamagnetic molybdenum matrix. The low-temperature magnetization exhibits steps at irregular field intervals, a result that cannot be explained using a Heisenberg model even if it is augmented by magnetic anisotropy and biquadratic terms. Allowing the exchange and anisotropy parameters to depend on the magnetic field provides the best fit to our data, suggesting that the molecular structure (and thus the interactions between spins) may be changing with applied magnetic field.

I. INTRODUCTION

Despite the enormous progress that has been made in understanding magnetic molecules over the past decade,[1,2,3,4,5,6,7,8,9] it is still a challenge to deduce the underlying microscopic spin Hamiltonian. Mn$_{12}$-acetate is a good example of this problem.[1,4,10,11,12,13] Although known for almost twenty years, only extensive investigation elucidated the model parameters.[14,15] Small magnetic molecules, with their simpler chemical and magnetic structure, can therefore provide an important opportunity to understand the dependence of magnetic observables on model parameters.[16,17,18]

In this work we report our joint experimental and theoretical efforts to understand the behavior of [Mo$_{12}^V$O$_{30}$(μ_2-OH)$_{10}$H$_2$\{Ni^{II}(H$_2$O)$_3$\}$_4$], henceforth abbreviated as {Ni$_4$Mo$_{12}$}, a magnetic molecule which is comprised of Ni^{II} centers positioned at the nucleophilic sites of an ϵ-Keggin cluster forming an almost ideal tetrahedron.[19] In contrast to several other nickel compounds which exhibit ferromagnetic[16,20,21,22,23] or mixed coupling,[24] the Ni centers of this molecule are antiferromagnetically coupled, as is also the case for certain Ni-2 × 2-grid molecules.[18] Because the structure of {Ni$_4$Mo$_{12}$} is almost perfectly tetrahedral one might anticipate that the magnetic energy levels are reasonably well described by an isotropic Heisenberg model with a single antiferromagnetic exchange parameter.[19] Such a Hamiltonian can be expressed in terms of the total spin:

$$\underset{\sim}{H} = -2J\sum_{u<v}\vec{\underset{\sim}{s}}(u)\cdot\vec{\underset{\sim}{s}}(v) + g\mu_B\vec{B}\cdot\sum_u\vec{\underset{\sim}{s}}(u) \quad (1)$$

$$= -J\left[\underset{\sim}{\vec{S}}^2 - 4s(s+1)\right] + g\mu_B B\,\underset{\sim}{S}_z \; ,$$

where $\vec{\underset{\sim}{s}}(u)$ is a single-spin operator at site u and $\vec{\underset{\sim}{S}}$ is the total spin operator. The spin quantum number of each Ni^{II} ion in an octahedral ligand field is $s = 1$. For antiferromagnetic coupling ($J < 0$) the resulting low-temperature magnetization curve $\mathcal{M}(B)$ that follows from (1) displays four steps before reaching saturation. These steps occur at the magnetic fields

$$B_{S\to(S+1)} = -\frac{2J}{g\mu_B}(S+1) \; , \qquad (2)$$

for $S = 0, 1, 2, 3$, where the lowest Zeeman-split levels of adjacent multiplets cross. In particular, from (2) it follows that the level crossing fields are uniformly spaced.[25,26] In stark contrast to the expectation of uniformly spaced crossing fields, the experimental magnetization $\mathcal{M}(B)$ curve of {Ni$_4$Mo$_{12}$} features non-equidistant steps at 4.5, 8.9, 20.1, and 32 T. Even assuming an anisotropic Hamiltonian[27] with two exchange

couplings and biquadratic terms as done for other Ni^{II}-compounds,[16,18] we were unable to account for the specific sequence of steps in the low-temperature magnetization of $\{Ni_4Mo_{12}\}$. In order to provide a comprehensive picture of the unusual high-field magnetic behavior of $\{Ni_4Mo_{12}\}$, we have been led to invoke field-dependent exchange and anisotropy parameters. We argue that this dependence emanates from changes in molecular structure (and thus the overlap of those atomic orbitals that determine the exchange interactions as well as the coordination geometries which affect the electronic single-ion properties) with applied magnetic field. The magneto-optical response of $\{Ni_4Mo_{12}\}$ supports a small change in the Ni^{II} coordination environment and the associated electronic single-ion properties.
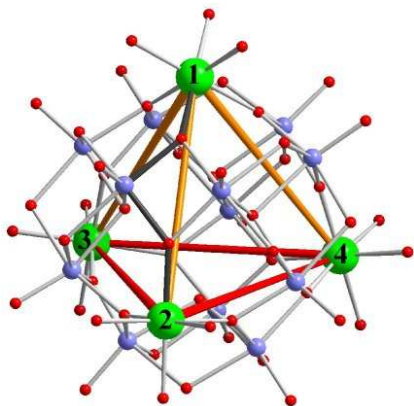
II. CHEMICAL AND CRYSTAL STRUCTURE

FIG. 1: (color online) Ball-and-stick representation of the $\{Ni_4Mo_{12}\}$ molecule (Ni: numbered big spheres; Mo: medium size spheres; O: small spheres; H: not shown) emphasizing a slightly stretched Ni$_4^{II}$ pyramid with a near-equilateral triangle base (Ni ions labeled 2, 3, and 4) and an elevated apex (Ni ion labeled 1). Ni-Ni distances: $d_{12} = 6.700(5)$ Å, $d_{13} = d_{14} = 6.689(1)$ Å, $d_{23} = d_{24} = 6.616(1)$ Å, $d_{34} = 6.604(1)$ Å.[19]

The neutral $\{Ni_4Mo_{12}\}$ cluster is isolated in the form of crystals of $[Mo_{12}^VO_{30}(\mu_2-OH)_{10}H_2\{Ni^{II}(H_2O)_3\}_4]\cdot 14\,H_2O$ and is based on the diamagnetic, highly-charged ϵ-Keggin anion $[Mo_{12}^VO_{38}(\mu_3-OH)_2]^{18-}$, built up from four edge-sharing $\{Mo_3\}$ groups (each consisting of three edge-sharing MoO_6 octahedra). Within the ϵ-Keggin framework, the Mo positions form six Mo_2^V groups with short Mo-Mo single bonds. The ϵ-Keggin structure is formally derived from the common α-Keggin isomer by rotating all four Mo_3 groups by $60°$, preserving the T_d symmetry. In $\{Ni_4Mo_{12}\}$, four $[Ni^{II}(H_2O)_3]^{2+}$ groups are coordinated each to three (unprotonated) μ_2-oxo centers that interlink the Mo positions of the Mo_2^V groups (Fig. 1). This results in a octahedral $O_3Ni^{II}(H_2O)_3$ coordination environment with all-trans-positioned oxo and

water ligands and nearly identical Ni-O distances (Ni-(μ_2-O): 2.05 Å, Ni-OH$_2$: 2.06 Å). This capping of the Mo_3 groups of the ϵ-Keggin fragment by four Ni^{II} positions produces a near-regular Ni$_4$ tetrahedron. Contrary to many other tetrahedral Ni$_4$ structures in which Ni pairs are connected by mononuclear bridging centers, in $\{Ni_4Mo_{12}\}$ each Ni pair is interconnected via one -O(-Mo-)$_2$O- bridging motif serving as a superexchange pathway (see Fig. 1 where one Ni-O-Mo-O-Ni pathway is highlighted by dark bonds). The geometry of each of these pathways is therefore characterized by four bond lengths, three bond angles, and two dihedral angles, as opposed to Ni$_4$-type structures comprising mononuclear linker groups (two bond lengths, one bond angle). Importantly however, the molecular geometry of $\{Ni_4Mo_{12}\}$ slightly deviates from the T_d-symmetric ideal, resulting in a slightly stretched Ni$_4$ pyramid with elongated Ni-Ni distances between the Ni positions of a basal Ni$_3$ plane and one apex. While the crystallographic symmetry operations result in the molecular point group C_s, the actual geometry is virtually of C_{3v} symmetry, and the geometric parameters for all Ni-O(-Mo-)$_2$O-Ni pathways correspondingly fall into two sets. Within these two sets, the individual bond lengths and angles display minimal deviations (typically < 0.8 %) from the respective averages: Intra-basal Ni-Ni contacts are characterized by $\langle$Ni-O$\rangle = 2.05$Å, $\langle$Mo-O$\rangle = 1.95$ Å, $\langle$Ni-O-Mo$\rangle = 135.4°$, and $\langle$Mo-O-Mo$\rangle = 89.6°$. For Ni-Ni contacts between the apex to the base positions average values of $\langle$Ni-O$\rangle = 2.03$ Å, $\langle$Mo-O$\rangle = 1.95$ Å, $\langle$Ni-O-Mo$\rangle = 137.9°$, and$\langle$¡Mo-O-Mo$\rangle = 94.6°$ are found. As the geometric parameters do not vary significantly within the intra-basal and within the apex-basal Ni-Ni contacts, we do not take into account slight deviations from the idealized C_{3v} symmetry, and use only exchange constants J and J' in this paper (see Fig. 2).
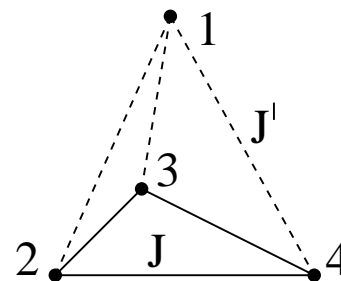

FIG. 2: Simplified structure of Ni$_4$: the superexchange interactions J' and J are represented by dashed and solid lines, respectively.

It should be added that magnetic exchange through polyoxomolybdates frameworks, especially if more than one possible pathway exists for each contact, has been found to be fairly insensitive to the separation distance of the pair of spin centers. Also, for similar systems based on mononuclear linker groups the bond angles have a

stronger effect on the exchange energies than the contact distance.[16,18,20,21,22,28,29,30] Due to the presence of crystal water molecules in the solid-state structure of $\{Ni_4Mo_{12}\}\cdot14\,H_2O$ which space the cluster entities apart, the closest intermolecular $Ni\cdots Ni$ distance in the solid state exceeds 7.15 Å, rendering inter-molecular (dipole-dipole) magnetic exchange insignificant.

III. EXPERIMENTAL RESULTS

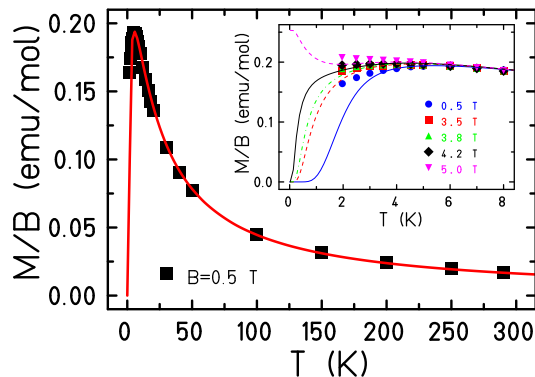### A. Magnetic properties of $\{Ni_4Mo_{12}\}$

FIG. 3: (color online) Low-field susceptibility: Experimental data are given by black squares whereas the solid curve shows the result assuming a simple Heisenberg Hamiltonian (1) with $J/k_B = -3.4$ K and an isotropic spectroscopic splitting factor $g = 2.25$. The inset shows a close-up view of the low-temperature region for different magnetic fields.
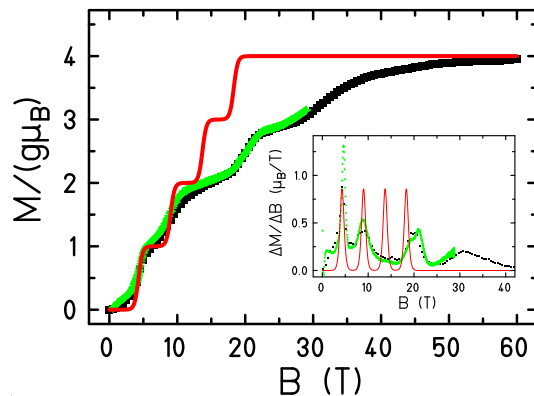

FIG. 4: (color online) Magnetization: Experimental data are given by squares (dark symbols – NHMFL, $T = 0.44$ K; light symbols – OHMFL, $T = 0.40$ K). The theoretical magnetization assuming a simple Heisenberg Hamiltonian (1) with $J/k_B = -3.4$ K and an isotropic spectroscopic splitting factor $g = 2.25$ is given by a solid curve for $T = 0.44$ K. The inset shows the experimental differential magnetization $d\mathcal{M}/dB$ as data points as well as the theoretical $d\mathcal{M}/dB$ (solid curve) using the same parameters as above.

Figure 3 displays the magnetic susceptibility $\mathcal{M}(B)$ of $\{Ni_4Mo_{12}\}$ as a function of temperature. These data were collected on a SQUID magnetometer (Quantum Design MPMS-5) at various magnetic fields in a temperature range of $2-290$ K. Using a simple Heisenberg Hamiltonian (1) one obtains $J/k_B = -3.4$ K and an isotropic g-factor of $g = 2.25$, see also Ref. 19. The model fit given by the solid curve in Fig. 3 is acceptable, although the low-temperature behavior is not well reproduced, as can be seen in the inset of Fig. 3, where the magnetic susceptibility for various field values and low temperatures is displayed. We suggest that the deviation is not only due to the presence of impurities but also due to anisotropic as well as biquadratic terms in the Hamiltonian which are known to be needed to model the low-temperature behavior of Ni^{II}-compounds.[16,18]

High-field magnetization measurements are a valuable tool to extract information on the spin Hamiltonian which is not accessible from magnetization measurements on commercial SQUID magnetometers. The high-field magnetization for a powder sample of $\{Ni_4Mo_{12}\}$ has been independently measured in pulsed magnetic fields at the facility of the National High Magnetic Field Laboratory (NHMFL) at Los Alamos as well as at the Okayama

High Magnetic Field Laboratory (OHMFL) by using a standard inductive method (maximum at NHMFL $B = 60$ T, whereas the maximum at OHMFL is $B = 40$ T, $dB/dt = 10000\ldots15000$ T/s). The results of these two measurements are in very close agreement. No hysteresis is found between up and down sweep runs, indicating thermal equilibrium behavior of $\mathcal{M}$ vs. B.

Figure 4 shows the magnetization as a function of applied external magnetic field at $T = 0.44$ K. Strikingly, four non-equidistant steps are observed in the magnetization. These steps are found near 4.5, 8.9, 20.1, and 32 T. Saturation of the magnetization is not observed until 60 T. For comparison, we show the expected response of a simple Heisenberg Hamiltonian (Eq. (1), ideal tetrahedron) for the model parameters extracted above. Note that this model predicts equidistant steps in the magnetization at 4.5, 9.0, 13.5, and 18.0 T with saturation above the fourth step. The drastic deviation between the predictions of Eqn. (1) and the experimental results cannot be the result of heating via the magnetocaloric effect. Although observed in other compounds, such an effect would only smear out the steps but not shift the step positions. In addition sample heating or cooling in a varying field is often accompanied by hysteresis, which is absent in this measurement.[46] The observed step positions thus constitute a challenge not only to the simple Heisenberg model given by (1), but also to more elaborate models (3) incorporating anisotropy terms and biquadratic exchange. We suggest that these models should be extended to include field-dependent parameters in order to account for our experimental results. This will be discussed in Sec. V.
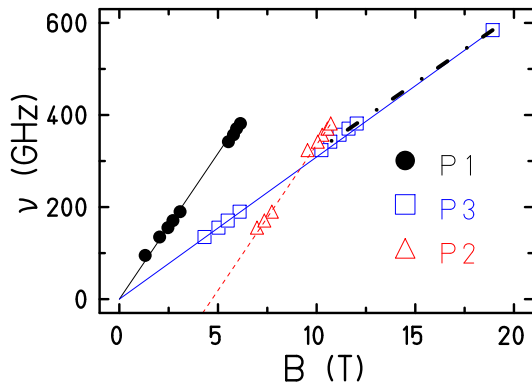
B. EPR response of {Ni$_4$Mo$_{12}$}

FIG. 5: (color online) The figure shows the dependence of the observed EPR resonance frequencies P1 (circles), P2 (triangles), and P3 (squares) on the magnetic field. The lines provide linear fits to the data. The data were taken at $T = 4.2$ K.

Figure 5 displays the results of our Electron Paramagnetic Resonance (EPR) measurements. The transmission of a powder sample was determined as a function of applied magnetic field in a frequency range from 95 GHz to 381.5 GHz. The figure shows the dependence of the observed EPR resonance frequencies P1 (circles), P2 (triangles), and P3 (squares) on magnetic field. One immediately notices that two different slopes can be assigned to the data, one corresponding to $\Delta M = 1$ and another one corresponding to forbidden transitions with $\Delta M = 2$. These dependencies can be qualitatively – and to some extent quantitatively – explained by looking at the Zeeman level scheme of the simple Heisenberg model (1) as it is schematically depicted in Fig. 6.
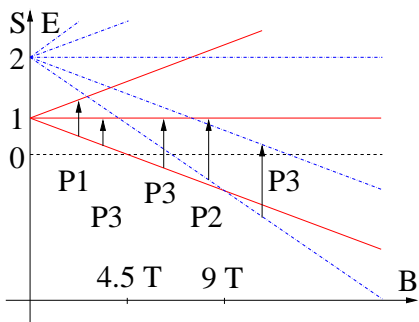

FIG. 6: (color online) The figure shows schematically the Zeeman level splittings in a pure Heisenberg model together with the assignments of allowed and forbidden transitions.

The strongest transition which we observe in the spectra is the allowed transition P3 with $\Delta M = 1$. Since the applied temperature is of the order of the coupling, this transition is actually a sum of several transitions. At low-field values it is dominated by the transition between

$(S = 1, M = -1)$ and $(S = 1, M = 0)$, whereas at higher fields the dominant contribution stems from the transition between $(S = 2, M = -2)$ and $(S = 2, M = -1)$. The dependence of the resonance frequency of P3 on the applied field suggests that the zero-field splitting in the triplet is small.

P1 is a low-field transition which connects $(S = 1, M = -1)$ and $(S = 1, M = +1)$ and thus should be forbidden. In the spectra its strength is much weaker than that of P3. We believe that this transition appears due to mixing of $\underset{\sim}{S}_z$ eigenstates that would arise from anisotropic contributions to the Hamiltonian. The line which is plotted through the data points suggests that the zero-field splitting between $(S = 1, M = -1)$ and $(S = 1, M = +1)$ is probably small, although, the experimental data points – which extend only down to 1.3 T – would also allow a somewhat bigger splitting, especially since the lowest-lying P1 data points appear to deviate from a straight line.

P2 is another rather weak forbidden transition which shares the slope with P1. We believe that this transition connects $(S = 2, M = -2)$ and $(S = 1, M = 0)$. This transition is not observable below about 7 T due to the fact that this transition occurs only when the mixing of $\underset{\sim}{S}_z$ eigenstates is sufficiently strong which is the case around the level crossing at 9 T. The dependence of this transition on temperature, i.e. on the thermal occupation of the level with $(S = 2, M = -2)$ is small. The extrapolation of the field dependence allows one to deduce an approximate isotropic Heisenberg coupling from the zero-field energy separation of the triplet and the pentuplet. From Eq. (1) one deduces that $E(S = 2) - E(S = 1) = -4J$, thus one obtains $J \approx -3.4$ K, which is in very good agreement with the exchange constants deduced from our susceptibility measurements. The spectroscopic splitting factor can be determined from the slopes of P3 and P1 in Fig. 5 to be $g = 2.23 \pm 0.03$, which is also in good agreement with the value deduced from the high-temperature behavior of the susceptibility. It is noteworthy that the high field data of transition P3 have a smaller slope which, if fitted alone (dashed-dotted line in Fig. 5), suggests $g \approx 2.11 \pm 0.03$. However, we want to point out that these considerations are done on the basis of the simple Heisenberg model (1), that does not take into account that a realistic Hamiltonian has to contain anisotropic terms. A more detailed explanation is given at the end of sec. V.

Summarizing this part, we find that the zero-field splitting is small. We explain this observation by the fact that the local principal axes of the Ni-ions point in different directions (radially outwards), and thus the average global anisotropy is small. Our use of a powder sample led to additional averaging.
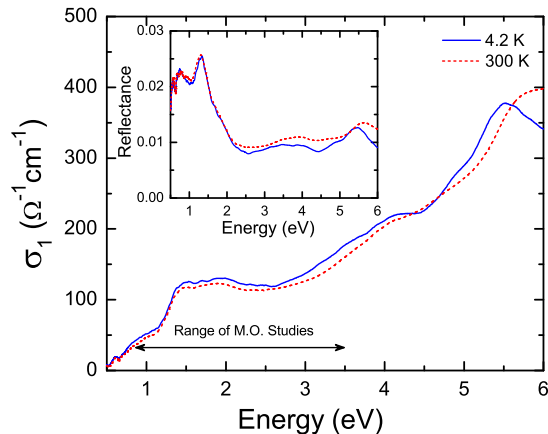
FIG. 7: (color online) Optical conductivity of a $\{Ni_4Mo_{12}\}$ pellet at 4.2 K (solid curve) and 300 K (dashed curve), calculated from reflectance measurements (inset) by Kramers-Kronig analysis. The energy range of our magneto-optical work is indicated by the arrow.

C. Optical properties of $\{Ni_4Mo_{12}\}$

Figure 7 displays the optical conductivity of $\{Ni_4Mo_{12}\}$. These experiments were carried out on a pressed powder sample using a Lambda-900 grating spectrometer equipped with reflectance stage and cryostat.[31] $\{Ni_4Mo_{12}\}$ is a semiconductor with an optical gap of ~ 0.6 eV. Based upon comparisons with chemically similar nicklates as well as existing electronic calculations,[32,33] we assign the excitations centered at 1.5 eV as on-site nickel d to d transitions, likely activated by modest hybridization with the coordinating oxygens. These excitations take place in both majority and minority channels according to recent DFT calculations.[33] The features above 3 eV are assigned as O p to Ni d charge transfer excitations. The energy range of our magneto-optical investigation is also shown in Fig. 7, providing a preview of the physical origin of the field-induced spectroscopic changes, discussed below.

Figure 8(a) displays the magneto-optical response of $\{Ni_4Mo_{12}\}$ as a function of magnetic field from 0 to 32 T at 4.2 K. These experiments were carried out on the same pressed powder sample using a grating spectrometer (0.8 - 3.5 eV) equipped with InGaAs and CCD detectors and a 33 T steady field resistive magnet at the NHMFL in Tallahassee, FL.[31] The reflectance ratio, $R(B)/R(B=0)$, is a normalized response and highlights changes in the optical properties with applied magnetic field. With increasing field, the reflectance of $\{Ni_4Mo_{12}\}$ decreases by $\sim 2\%$. It is notable that this effect occurs in the visible spectral range, hence the name "magnetochromism". Based upon the aforementioned peak assignments in the optical conductivity spectrum in Fig. 7 and the $\sigma_1(B)/\sigma_1(B=0$ T) ratio data in the inset of Fig. 8(b), we attribute the observed magnetochromic effect to a field-induced modification of the Ni d to d on-site excitation. Distortion of
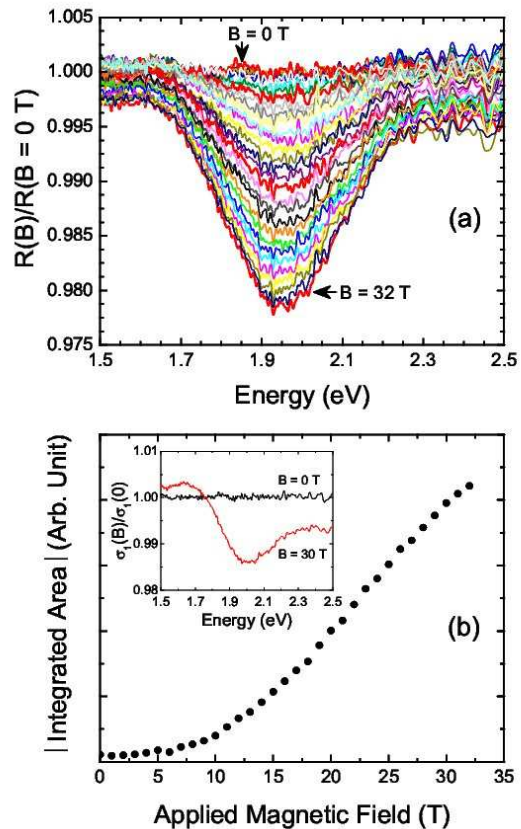

FIG. 8: (color online) (a) The normalized magneto-optical response, $R(B)/R(B=0$ T), of $\{Ni_4Mo_{12}\}$ pressed powder in an applied magnetic field from 0 to 32 T at 4.2 K. 1 T steps are shown. No hysteresis is observed. (b) Absolute value of the integrated area of the magneto-optical reflectance ratio feature as a function of applied magnetic field (solid symbol). Results from the integrated optical conductivity data are similar. The inset shows the change in the optical conductivity of $\{Ni_4Mo_{12}\}$ with magnetic field, $\sigma_1(B=30$ T$)/\sigma_1(B=0$ T). The $B=0$ T curve ratios data taken before and after the field sweep, giving an indication of overall spectral reproducibility.

the pseudo-octahedral Ni^{II} crystal field environment is a plausible driver. Note that this is a local, molecular-level distortion rather than a bulk effect. No field-induced changes were observed on the leading edge of the O p to Ni d charge transfer bands above 3 eV.

We quantify the magneto-optical effect in $\{Ni_4Mo_{12}\}$ by plotting the absolute value of the integrated intensity of the reflectance ratio as a function of applied magnetic field (Fig. 8(b)).[47] The magneto-optical effect is small at low fields, becomes appreciable above 10 T, and continues to grow for $B \geq 30$ T. There is no evidence of saturation to 33 T. The overall rising magnetochromic response can be fit with several different functions including a cubic polynomial in $|B|$ and a simple exponential, suggesting a likely functional form for the field-dependence of the magnetic parameters in $\{Ni_4Mo_{12}\}$, described below. We propose that the applied magnetic field interacts with the spin centers, deforming the local structure around

the Ni^{II} sites. This process modifies the crystal field environment, the result of which is a field-induced change in electronic structure (Fig. 8 (a)). Thus, these spectroscopic results support the picture of field-dependent exchange and anisotropy terms in the spin Hamiltonian of {Ni$_4$Mo$_{12}$} that derive from magnetoelastic (and consequent spin-orbit) interactions. Magneto-optical effects due to field-induced changes in local structure have also been observed in other materials including (CPA)$_2$CuBr$_4$ and K$_2$V$_3$O$_8$.[34,35]

IV. THEORETICAL MODELS

In order to understand the magnetic properties of {Ni$_4$Mo$_{12}$} we adopt the following general Hamiltonian that has been used for other Ni^{II}-compounds,[16,18]

$$\underset{\sim}{H} = \underset{\sim}{H}_H + \underset{\sim}{H}_{ani} + \underset{\sim}{H}_{biq} + \underset{\sim}{H}_Z \ , \ \text{where} \quad (3)$$

$$\underset{\sim}{H}_H = -2\sum_{u<v} J_{uv}\,\underset{\sim}{\vec{s}}(u)\cdot\underset{\sim}{\vec{s}}(v) \quad (4)$$

$$\underset{\sim}{H}_{ani} = D\left[\sum_u \left(\vec{e}_r(u)\cdot\underset{\sim}{\vec{s}}(u)\right)^2 - \frac{8}{3}\right] \quad (5)$$

$$\underset{\sim}{H}_{biq} = -2\sum_{u<v} j_{uv}\left(\underset{\sim}{\vec{s}}(u)\cdot\underset{\sim}{\vec{s}}(v)\right)^2 \quad (6)$$

$$\underset{\sim}{H}_Z = g\,\mu_B\,\vec{B}\cdot\sum_u \underset{\sim}{\vec{s}}(u) \ . \quad (7)$$

Here $\underset{\sim}{H}_H$ denotes the Heisenberg Hamiltonian and $\underset{\sim}{H}_{ani}$ describes the single-site anisotropic (ligand field) contribution, which is compatible with the approximate tetrahedral symmetry of {Ni$_4$Mo$_{12}$}. The unit vector $\vec{e}_r(u)$, which points radially outwards, serves as a local anisotropy axis for site u. The term $8/3$ is convenient in order to render the Hamiltonian traceless. $\underset{\sim}{H}_{biq}$ represents biquadratic terms, which are the next higher order compared to the Heisenberg Hamiltonian,[36] and $\underset{\sim}{H}_Z$ is the Zeeman term. We employ a single spectroscopic splitting factor g since the g-tensor anisotropy was found to be very small for the present system; a similar result has been found for Ni^{II} squares.[18] We also assume that a possible anisotropic exchange between the Ni^{II} centers is small because the orbital contribution to the ground state is small.[37]

In the following sections, we simplify $J_{uv} = J$ and $j_{uv} = j$, or, if we use two different constants, $J' = J_{12} = J_{13} = J_{14}$, $J = J_{23} = J_{24} = J_{34}$ and $j' = j_{12} = j_{13} = j_{14}$, $j = j_{23} = j_{24} = j_{34}$, as illustrated in Fig. 2. We also account for impurity effects (additional paramagnetic Ni^{II} ions) and their batch-to-batch variation by adding a paramagnetic term to the Hamiltonian (3).

We have made numerous attempts to model the experimental magnetization curve of {Ni$_4$Mo$_{12}$} (Fig. 4) with field-independent values of J and D, as described previously. Despite these efforts, an explanation for the non-

uniform spacing of the crossing fields has not been forthcoming. Assuming a Hamiltonian with two exchange couplings and anisotropic as well as biquadratic terms as given in (3) did not result in a satisfactory description of all magnetic observables on a common footing.[27] Therefore, we extended our model to allow J and D to vary with applied magnetic field. The possible field-induced distortion of the crystal field environment around the Ni centers motivates this ansatz.

V. FIELD-DEPENDENT MODEL PARAMETERS

A. Low-field properties of {Ni$_4$Mo$_{12}$}

It is not *a priori* clear how the model parameters should depend on the magnetic field since this dependence is indirect. The exchange couplings, the biquadratic contributions as well as the anisotropy result from the electronic structure, and are (complicated) functions of orbital overlaps, lattice stiffness, and spin-orbit coupling. If the electronic structure is noticeably altered by an applied field it is probable that the parameters entering Hamiltonian (3) are also changed, but very likely in a highly non-linear manner. To the best of our knowledge, so far such dependencies were only observed in certain Mn grid molecules,[38] where the anisotropy changes sign at a level crossing. It appears plausible to us that besides continuous variations, the parameters can also change abruptly since the molecular structure may relax into new ground states at certain field values. Therefore, one can anticipate that the field-dependence of the model parameters might only be piecewise analytic between the abrupt changes. In this section we therefore investigate simple piecewise parameterizations of the Hamiltonian. We also neglect a possible anisotropic field dependence of the parameters, i.e. the exchange parameters of different bonds would be modified differently, and therefore the effect should depend on the relative orientation of the molecule with respect to the field.

It turns out that the low-field susceptibility versus temperature data, shown in Fig. 9, can be modeled by two sets of parameters. The magnetization of two different samples of {Ni$_4$Mo$_{12}$} at $B = 0.5$ T can be understood assuming $J/k_B = -3.2$ K, $J'/k_B = -3.2$ K, $j/k_B = 1.6$ K, $j' = 0$, $D/k_B = -1.0$ K together with the separate term to account for the paramagnetic impurities (free Ni^{II} ions) contained in the samples (parameterization **1**). The parameters of the Hamiltonian compare nicely to those of 2×2–Ni^{II} grid molecules.[18] The sign of the anisotropy as well as that of the biquadratic term signal the same behavior, only the absolute value of the biquadratic term is somewhat larger. The resulting zero-field splitting of the triplet is only 0.15 K, in very good agreement with our EPR results. The fact that the biquadratic term is one order of magnitude larger than usually observed ($j \propto J/100$)[18,36,39] signals that
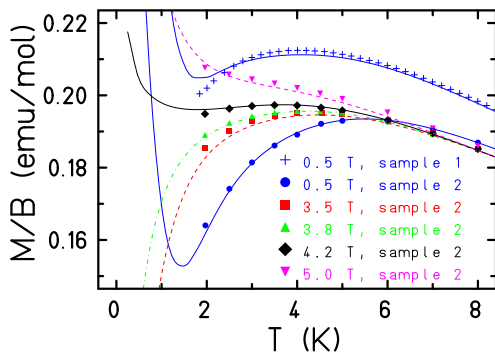
FIG. 9: (color online) Low-field susceptibility: The measured data are given by symbols. The fits for $B = 0.5$ T are obtained using $J/k_B = -3.2$ K, $J'/k_B = -3.1$ K, $j/k_B = 1.6$ K, $j'/k_B = 0$, $D/k_B = -1.0$ K. The data for field values of $B = 3.5$ T up to 5 T are approximated using $J/K = -3.2$ K, $J'/k_B = -3.2$ K, $j/k_B = 1.5$ K, $j'/k_B = 0$, and $D/k_B = -3.2$ K. $g = 2.195$ in all cases. The estimated impurity concentrations are 0.216 and 0.146 individual Ni^{II} ions per $\{Ni_4Mo_{12}\}$ molecule for sample 1 and 2, respectively. The simulated data are averaged over 100 orientations.

the bonds in the basal triangle of the molecule might be rather soft. The other four susceptibility measurements, Fig. 9, which are obtained from $B = 3.5$ T to 5 T, can be better approximated by a second set of parameters: $J/k_B = -3.2$ K, $J'/k_B = -3.1$ K, $j/k_B = 1.5$ K, $j'/k_B = 0$, and $D/k_B = -3.2$ K (parameterization **2**). These parameters differ from those for $B = 0.5$ T in two ways: (1) the biquadratic contribution is 7 % smaller, (2) the anisotropy coefficient is three times larger.

B. High-field properties of $\{Ni_4Mo_{12}\}$

Although the above parameterization describes the low-field data up to $B \approx 5$ T reasonably well, it fails to reproduce the magnetization data at higher fields. The dramatic increase of the field spacings between adjacent magnetization steps at 4.5, 8.9, 20.1, and 32 T cannot be explained by small changes of the anisotropy D or the coupling J. The third field spacing is about twice the first one, which using relation (2) suggests an exchange coupling that is about 1.25 of the original one. In the following we therefore investigate a model where only the exchange parameters are allowed to depend on field. This is of course a simplification since all parameters of the Hamiltonian (J, j, D, and g) should be modified in a varying field. For our purpose we assume a hypothetical exponential dependence of J on the absolute value of the external magnetic field

$$J(B) = J_0 \exp\left(\frac{|B|}{\gamma}\right), \qquad (8)$$

which we motivate by a possible change of the overlap of those orbitals that are involved in the superex-

change. Such a change could be caused by variations of the bond distances and angles; the latter are known to have dramatic effects on the exchange parameters. Based on the magneto-structural correlations for Ni-O cubanes in Ref. 28, a change of the exchange parameter in $\{Ni_4Mo_{12}\}$ by the necessary amount would correspond to a change of the bond angles by approximately one quarter of a degree if the effect was attributed solely to bond angle modifications. A literature survey of chemically-similar Ni(II) cluster compounds[16,18,20,21,22,28,29,30] reveals that J and D vary from at least -10 to 17.5 cm^{-1} (-7 to 12.2 K) and -5.5 to 0.5 cm^{-1} (-3.8 to 8.5 K), respectively. In these systems, bond angle is the governing structural parameter due to the intimate relationship between angle and magnetic orbital overlap.[48] There is a linear correlation between the value of J and Ni-O-Ni and Ni-O-O-Ni bond angles in several nickel clusters. Although the transition metal centers in these nickel clusters have different local environments, the aforementioned range of J and D represents the variation in physical parameters that can be accessed by chemical tuning in these compounds. Magnetic field-induced effects are anticipated to be in this range as well.
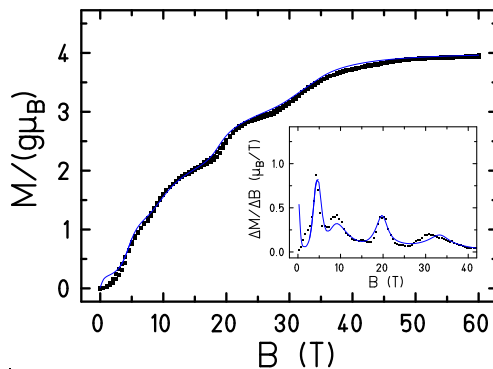

FIG. 10: (color online) Magnetization of sample 2: Experimental data (NHMFL) are given by squares. The solid curve provides the best fit using a Hamiltonian with an exponentially field-dependent coupling. The simulated data are averaged over 100 orientations. The inset shows the experimental differential magnetization $d\mathcal{M}/dB$ as data points as well as the theoretical $d\mathcal{M}/dB$ (solid curve) using the same parameters as above.

The best fit using two exchange parameters was obtained for $J/k_B = -4.2$ K $* \exp(B/96$ T), $J'/k_B = -3.2$ K $* \exp(B/52$ T), $j/k_B = 0.16$ K, $j'/k_B = 0.39$ K, $D/k_B = -8.9$ K, and $g = 2.195$ together with the paramagnetic impurity contribution already determined for sample 2 (parameterization **3**). This fit is shown in Fig. 10. Except for small fields, where the two aforementioned parameter sets are appropriate, this model provides a rather good description of the magnetization over a large field range. The assumption of an exponential dependence is not essential; a polynomial dependence yields similar results.

C. EPR revisited

The level scheme and possible EPR transitions can be shown more closely using the parameters of the general Hamiltonian (3).
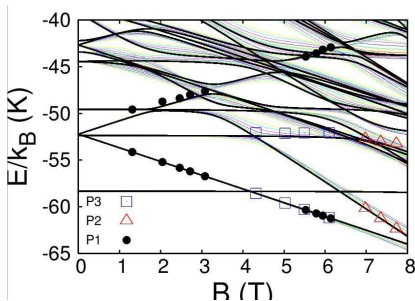

FIG. 11: (color online) The figure shows the Zeeman level splittings for the realistic Heisenberg model (3) (parametrization **2**) for several orientations of the field relative to the molecules. The various curves, which differ especially at avoided level crossings, represent relative angles of $10°$.

In Fig. 11 the Zeeman split levels are presented for fields up to 8 T using parametrization **2**. The thick curves show levels for an orientation of the field axis pointing from the mid point of the basal triangle through the top Ni center (Ni ion 1 in Fig. 2). The thinner curves show the levels for orientations with relative angle steps of $10°$ along a great circle through one of the basal Ni centers. The variation of the level positions with orientation for a fixed absolute value of the external field is especially large at avoided level crossings. Although the final EPR line is given by averaging over all orientations one can already deduce from Fig. 11 that the EPR measurement is in full agreement with the microscopic Hamiltonian. The attached symbols for the three observed transitions match the calculated level spacings very well.
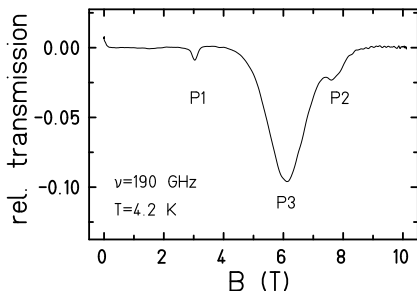

FIG. 12: Relative EPR transmission observed at $\nu = 190$ GHz, which corresponds to an energy level difference of 9.12 K.: The dominant (allowed) transition P3 is rather broad, whereas the the weaker (forbidden) transition P1 results in a much sharper peak. The other weak (forbidden) transition P2, which is masked by P3, is broader than P1.

To some extent one can even explain the widths of the

three transitions, which are shown in Fig. 12 for a frequency of $\nu = 190$ GHz and a temperature of $T = 4.2$ K. The transition P1, which occurs between energy levels marked by filled circles in Fig. 11, is rather narrow; this is connected to the fact that variations of the field direction do not lead to strong variations of the respective levels. This also implies that the mixing of $\underset{\sim}{S}_z$ eigenstates is weak and thus the amplitude of this forbidden transition is small. P3 on the contrary is an allowed transition which dominates the spectrum. In the investigated field range it is given mainly by the transition between levels marked by open squares in Fig. 11, but transitions between other (unmarked) levels also contribute. he rather broad line can in part be explained by the rather strong variation of the upper marked level with variations of the field direction. The transition P2 between levels marked by open triangles in Fig. 11 is stronger than P1 but also broader, which can again be understood by looking at the variation of levels.

VI. CONCLUSIONS

We have presented a comprehensive experimental and theoretical investigation of the magnetic molecule $\{Ni_4Mo_{12}\}$. We find that the main model parameters of the Hamiltonian (i.e. exchange and anisotropy parameters) have a strong dependence on magnetic field, an effect that may be accompanied by molecular magnetostriction. All of our efforts to avoid this conclusion lead to a blatant contradiction between theory and experiment. The discovery of a dependence of Hamiltonian parameters on field in $\{Ni_4Mo_{12}\}$ is quite novel. Nevertheless, it may be a general characteristic of magnetic cluster-based materials with strong lattice coupling. It is well known that most materials (including magnetic molecules) are not rigid.[34,35,40,41,42] In addition, only relatively few high-field magnetization studies have been performed to date. Thus, it is of interest to discover whether other magnetic molecules might display a similarly strong dependence of the model parameters on magnetic field in the regime above 20 T.

[*] Electronic address: jschnack@uos.de

[1] R. Sessoli, D. Gatteschi, A. Caneschi, and M. A. Novak, Nature **365**, 141 (1993).

[2] D. Gatteschi, A. Caneschi, L. Pardi, and R. Sessoli, Science **265**, 1054 (1994).

[3] D. Gatteschi, Adv. Mater. **6**, 635 (1994).

[4] E. Coronado, P. Delhaes, D. Gatteschi, and J. Miller, eds., *Localized and Itinerant Molecular Magnetism: From Molecular Assemblies to the Devices*, vol. 321 of *NATO Advanced Studies Institute, Series E: Applied Sciences* (Kluwer Academic, Dordrecht, 1996).

[5] A. Caneschi, D. Gatteschi, C. Sangregorio, R. Sessoli, L. Sorace, A. Cornia, M. A. Novak, C. Paulsen, and W. Wernsdorfer, J. Magn. Magn. Mater. **200**, 182 (1999).

[6] O. Waldmann, J. Schülein, R. Koch, P. Müller, I. Bernt, R. W. Saalfrank, H. P. Andres, H. U. Güdel, and P. Allenspach, Inorg. Chem. **38**, 5879 (1999).

[7] A. Müller, M. Luban, C. Schröder, R. Modler, P. Kögerler, M. Axenovich, J. Schnack, P. C. Canfield, S. Bud'ko, and N. Harrison, Chem. Phys. Chem. **2**, 517 (2001).

[8] W. Wernsdorfer, N. Aliaga-Alcalde, D. N. Hendrickson, and G. Christou, Nature **416**, 406 (2002).

[9] A. Müller, P. Kögerler, and A. W. M. Dress, Coord. Chem. Rev. **222**, 193 (2001).

[10] T. Lis, Acta Chrytallogr. B **36**, 2042 (1980).

[11] L. Thomas, F. Lionti, R. Ballou, D. Gatteschi, R. Sessoli, and B. Barbara, Nature **383**, 145 (1996).

[12] Z. H. Jang, A. Lascialfari, F. Borsa, and D. Gatteschi, Phys. Rev. Lett. **84**, 2977 (2000).

[13] Y. Furukawa, K. Watanabe, K. Kumagai, F. Borsa, and D. Gatteschi, Phys. Rev. B **64**, 104401 (2001).

[14] N. Regnault, T. Jolicœur, R. Sessoli, D. Gatteschi, and M. Verdaguer, Phys. Rev. B **66**, 054409 (2002).

[15] G. Chaboussant, A. Sieber, S. Ochsenbein, H.-U. Güdel, M. Murrie, A. Honecker, N. Fukushima, and B. Normand, Phys. Rev. B **70**, 104422 (2004).

[16] R. Koch, O. Waldmann, P. Müller, U. Reimann, and R. W. Saalfrank, Phys. Rev. B **67**, 094407 (2003).

[17] M. Luban, F. Borsa, S. Bud'ko, P. Canfield, S. Jun, J. Jung, P. Kögerler, D. Mentrup, A. Müller, R. Modler, et al., Phys. Rev. B **66**, 054407 (2003).

[18] O. Waldmann, J. Hassmann, P. Müller, D. Volkmer, U. S. Schubert, and J. M. Lehn, Phys. Rev. B **58**, 3277 (1998).

[19] A. Müller, C. Beugholt, P. Kögerler, H. Bogge, S. Bud'ko, and M. Luban, Inorg. Chem. **39**, 5176 (2000).

[20] H. Andres, R. Basler, A. J. Blake, C. Cadiou, G. Chaboussant, C. M. Grant, H. U. Gudel, M. Murrie, S. Parsons, C. Paulsen, et al., Chem. Eur. J. **8**, 4867 (2002).

[21] E. C. Yang, W. Wernsdorfer, S. Hill, R. S. Edwards, M. Nakano, S. Maccagnano, L. Zakharov, A. Rheingold, G. Christou, and D. N. Hendrickson, Polyhedron **22**, 1727 (2003).

[22] M. Moragues-Canovas, M. Helliwell, L. Ricard, E. Riviere, W. Wernsdorfer, E. Brechin, and T. Mallah, Eur. J. Inorg. Chem. pp. 2219–2222 (2004).

[23] P. King, R. Clerac, W. Wernsdorfer, C. E. Anson, and A. K. Powell, Dalton Trans. pp. 2670–2676 (2004).

[24] S. Demeshko, G. Leibeling, W. Maringgele, F. Meyer, C. Mennerich, H. H. Klauss, and H. Pritzkow, Inorg. Chem. **44**, 519 (2005).

[25] G. L. Abbati, A. Caneschi, A. Cornia, A. C. Fabretti, and D. Gatteschi, Inorg. Chim. Acta **297**, 291 (2000).

[26] J. Schnack and M. Luban, Phys. Rev. B **63**, 014418 (2001).

[27] M. Brüger, diploma thesis, Universität Osnabrück, Universität Osnabrück (2003).

[28] M. A. Halcrow, J.-S. Sun, J. C. Huffman, and G. Christou, Inorg. Chem. **34**, 4167 (1995).

[29] A. Escuer, M. Font-Bardìa, S. B. Kumar, X. Solans, and R. Vicente, Polyhedron **18**, 909 (1999).

[30] C. Cadiou, M. Murrie, C. Paulsen, V. Villar, W. Wernsdorfer, and R. Winpenny, Chem. Commun. pp. 2666–2667 (2001).

[31] J. Choi, J. D. Woodward, J. L. Musfeldt, X. Wei, M. H. Whangbo, J. He, R. Jin, and D. Mandrus, Phys. Rev. B **70**, 085107 (2004).

[32] K. Park, E.-C. Yang, and D. N. Hendrickson, J. Appl. Phys. **97**, 10M522 (2005).

[33] A. V. Postnikov, M. Brüger, and J. Schnack, Phase Transitions **78**, 47 (2005).

[34] J. D. Woodward, J. Choi, J. L. Musfeldt, J. T. Haraldsen, X. Wei, H.-J. Koo, D. Dai, M.-H. Whangbo, C. P. Landee, and M. M. Turnbull, Phys. Rev. B **71**, 174416 (2005).

[35] R. Rai, J. Cao, J. Musfeldt, X. Wei, D. Singh, B. Sales, and D. Mandrus, submitted.

[36] A. Bencini and D. Gatteschi, *Electron parametric resonance of exchange coupled systems* (Springer, Berlin, Heidelberg, 1990).

[37] R. Basler, C. Boskovic, G. Chaboussant, H. U. Gudel, M. Murrie, S. T. Ochsenbein, and A. Sieber, ChemPhysChem **4**, 910 (2003).

[38] O. Waldmann, L. Zhao, and L. Thompson, Phys. Rev. Lett. **88**, 066401 (2002).

[39] N. L. Huang and R. Orbach, Phys. Rev. Lett. **12**, 275 (1964).

[40] A. B. Sushkov, J. L. Musfeldt, Y. J. Wang, R. M. Achey, and N. S. Dalal, Phys. Rev. B **66**, 144430 (2002).

[41] R. W. Saalfrank, B. Demleitner, H. Glaser, H. Maid, D. Bathelt, F. Hampel, W. Bauer, and M. Teichert, Chem.-Eur. J. **8**, 2679 (2002).

[42] R. W. Saalfrank, C. Deutscher, H. Maid, A. M. Ako, S. Sperner, T. Nakajima, W. Bauer, F. Hampel, B. A. Hess, N. J. R. V. Hommes, et al., Chem.-Eur. J. **10**, 1899 (2004).

[43] I. Chiorescu, W. Wernsdorfer, A. Müller, H. Bögge, and B. Barbara, Phys. Rev. Lett. **84**, 3454 (2000).

[44] O. Waldmann, R. Koch, S. Schromm, P. Müller, I. Bernt, and R. W. Saalfrank, Phys. Rev. Lett. **89**, 246401 (2002).

[45] O. Waldmann, R. Koch, S. Schromm, P. Müller, I. Bernt, and R. W. Saalfrank, Phys. Rev. Lett. **90**, 229904 (2003).

[46] The interested reader is referred to the extensive literature on "butterfly hysteresis loops" in molecular magnets, e.g. Refs. 43,44,45.

[47] Similar results are obtained using the optical conductivity ratio, $\sigma_1(B)/\sigma_1(0)$.

[48] In contrast, the Ni..Ni distances have only a small effect on the observed values of J.